ACS Catalysis

Research Article

pubs.acs.org/acscatalysis

Hydrogenation of CO_2 over Ru/YSZ Electropromoted Catalysts

D. Theleritis,[†] S. Souentie,[†,*] A. Siokou,[‡] A. Katsaounis,[†] and C. G. Vayenas[†,§,*]

[†]Department of Chemical Engineering, University of Patras, Caratheodory 1 St, GR-26504 Patras, Greece

[‡]Institute of Chemical Engineering and High Temperature Chemical Processes (FORTH/CE-HT), Foundation for Research and Technology Hellas, 26504 Patras, Greece

[§]Division of Natural Sciences, Academy of Athens, Panepistimiou 28 Avenue, GR-10679 Athens, Greece

ABSTRACT: The effect of electrochemical promotion of catalysis (EPOC or NEMCA effect) was investigated for the hydrogenation of CO_2 using Ru catalyst electrodes supported on YSZ solid electrolyte pellets at temperatures 200−300 °C and ambient pressure. Methane was found to be the main reaction product at temperatures up to 240 °C, whereas CO dominated at higher temperatures. It was found that the O^{2-} supply to the Ru surface causes a significant increase in the CH_4 formation rate and selectivity, accompanied by a significant decrease in the rate of CO formation. This is a very rare case in which electrochemical promotion is found to promote a catalytic reaction and at the same time to poison a reaction proceeding in parallel with the promoted one. The faradic efficiency values were found to be on the order of $10-10^3$, which are among the highest reported in the EPOC hydrogenation literature. The kinetic and electropromotion results can be interpreted, using the rules of electrochemical promotion, in terms of the changes in the surface RuO_x/Ru ratio induced via potential application, as observed via ex situ XPS.

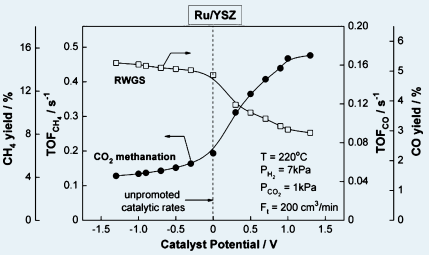

KEYWORDS: *CO_2 hydrogenation, methanation, Ru electrodes, EPOC, NEMCA*

1. INTRODUCTION

The hydrogenation of CO_2 to hydrocarbons, alcohols, or both has received great attention worldwide in recent years, both as a potential source of renewable fuels and as a potential means of decreasing the overall CO_2 emissions.

Most studies of the catalytic hydrogenation of CO_2 have been performed in fixed-bed reactors using mainly metal catalysts (e.g., Pt, Rh, Pd, Ru, Cu, Fe, Co, Ni) supported over several metal oxide supports (e.g., Nb_2O_3, ZrO_2, Al_2O_3, SiO_2).[1−22] High pressure operation conditions (5−70 atm) are often used to increase the thermodynamic equilibrium conversion to light hydrocarbons or methanol.[6,23−28]

When CO_2 and H_2 are co-fed over a hydrogenation catalyst, there are two main processes that can take place:

$$CO_2 + H_2 \rightarrow CO + H_2O \quad (1)$$

$$xCO_2 + (2x - z + y/2)H_2 \rightarrow C_xH_yO_z + (2x - z)H_2O \quad (2)$$

The former is the reverse water−gas shift reaction (RWGS), which is a redox reaction, and the latter is a synthesis reaction leading to the formation of hydrocarbons, alcohols, or both. For example, the methanation reaction can be described by eq 2 for $x = 1$, $y = 4$, and $z = 0$, whereas for $x = 1$, $y = 4$, and $z = 1$, one has the methanol synthesis reaction.

The intermediate compounds and the rate-determining step of the CO_2 methanation reaction over noble metal catalysts, including Ru, are still under discussion. Earlier studies[26,28−30] proposed a direct CO_2 methanation mechanism; however, nowadays, it is generally accepted that adsorbed CO, denoted CO_{ad} and originating from CO_2 dissociative adsorption, is the main reaction intermediate. This CO_{ad} species is believed to be present in the case of both the CO and the CO_2 methanation mechanisms. In the case of CO methanation, recent studies have proposed that CO_{ad} interacts with H_{ad} toward formyl adspecies (CH_xO), followed by hydrogen-assisted scission of the C−O bond and further hydrogenation to methane.[14,17,31]

In the case of CO_2 methanation, some research groups[2−5,13,14,17,32−37] believe that the CO_{ad} species that are present on the catalyst surface follow the same mechanism as CO methanation, as mentioned above. Another point of view has been offered[15,16,38] in which CH_xO was not observed. They proposed that the mechanism of CO_2 methanation proceeds via CO_{ad} dissociation, followed by hydrogenation of adsorbed carbon species.

The chemical promotion of the CO_2 methanation catalysts by alkalis has also been investigated by several groups.[9,11,20,26,37,39] Yaccato et al.[11] reported that when Ru is doped with alkaline metal electropositive promoters, a decrease in the methanation activity is observed. They also reported that Na doping of Co enhances the RWGS reaction rate.

A parallel approach to classical chemical promotion is the use of electrochemical promotion of catalysis (EPOC or nonfaradic electrochemical modification of catalytic activity, NEMCA effect[40]) to electrochemically promote metal catalyst electrodes

Special Issue: Electrocatalysis

Received: January 30, 2012
Revised: March 9, 2012
Published: March 16, 2012

deposited over solid electrolyte supports, for example, YSZ, TiO_2, or CeO_2.

The phenomenon of electrochemical promotion of catalysis has been extensively investigated in the last 30 years for more than 90 catalytic reaction systems using a variety of metal catalysts (or conductive metal oxides), solid electrolytes, and catalytic reactions.[40−54] In EPOC studies, the conductive catalyst electrode is in contact with an ionic conductor ceramic support, and the catalyst (e.g., noble metals and oxides) is electrochemically promoted by applying a current or potential between the catalyst film and a counter or reference electrode, respectively.

Numerous surface science and electrochemical techniques have shown that EPOC is due to electrochemically controlled migration (reverse spillover or backspillover) of promoting ionic species (O^{2-} in the case of YSZ, TiO_2 and CeO_2; Na^+ or K^+ in the case of β''-Al_2O_3, protons in the case of Nafion, CZI ($CaZr_{0.9}In_{0.1}O_{3-\alpha}$) and BCN18 ($Ba_3Ca_{1.18}Nb_{1.82}O_{9-\alpha}$), etc.) between the ionic or mixed ionic−electronic conductor support and the gas-exposed catalyst surface, through the catalyst−gas−electrolyte three-phase boundaries (tpb).[40,52,53,55,56]

When YSZ is used as the solid electrolyte, promoting ionic species (denoted $O^{\delta-}-\delta^+$) are generated in an electrochemical step at the tpb (eq 3) and then spread, due to strong repulsive dipole−dipole interactions, over the entire metal−gas interface, establishing there an overall neutral effective double layer,[40]

$$O^{2-}(YSZ) + Ru \rightarrow [O^{\delta-} - \delta^+]Ru + 2e^- \quad (3)$$

at a rate $I/2F$, where I is the current and F Faraday's constant.

These promoting $O^{\delta-}$ species are more strongly bonded to the catalytic surface than normally adsorbed oxygen.[40] It should be noted that the backspillover species are overall neutral since the anionic oxygen species $O^{\delta-}$ is accompanied by its image charge δ^+ in the metal. They only differ from normally adsorbed oxygen in the dipole moment (∼2 vs ∼1 D) and not in the total charge, which is zero in both cases.[40,57]

In EPOC studies under reducing conditions,[58−60] as in the present case, it is likely that the promoting anionic species is a hydroxyl group formed via

$$O^{2-}(YSZ) + Ru + (1/2)H_2 \rightarrow [OH^{\zeta-} - \zeta^+]Ru + 2e^- \quad (4)$$

The electrochemical promotion of the hydrogenation of CO_2 has been studied in the past over Cu,[60] Rh,[60,61] Pt,[60,62] and carbon nanofiber (CNF)-supported Ni and Ru[63] catalyst electrodes deposited over YSZ. In the case of Pt catalyst films, only CO formation was observed.[60,62] In ref 60, where Cu/YSZ catalyst films were used, CO, CH_4, and C_2H_4 were produced, and an electrophilic behavior was observed for all three products. In general, when Rh catalyst films were used, CO and CH_4 were produced at temperatures of 340−480 °C.[60,61] When a CNF−Ru catalyst was used,[63] CH_4 and CO were produced, but only negative polarization was found to result in CH_4 formation rate increase.

When Pd catalyst films were deposited on β''-Al_2O_3, a K^+ ionic ceramic conductor support,[64] the catalytic activity was limited to temperatures above 530 °C, where only CO was produced. Moreover, when Cu catalyst films were deposited on $SrZr_{0.90}Y_{0.10}O_{3-\alpha}$, a high temperature proton conductor support, only CO was detected at temperatures 550−750 °C.

In the present study the effect of catalyst potential on the catalytic activity and selectivity of the CO_2 methanation (eq 2) and the RWGS (eq 1) reactions was investigated using Ru catalyst films deposited over YSZ solid electrolyte pellets at temperatures 200 to 300 °C and ambient pressure.

2. EXPERIMENTAL SECTION

2.1. Catalyst Preparation. The solid electrolyte was a pellet of 8 mol % Y_2O_3-stabilized ZrO_2 (YSZ) of 18 mm diameter and 2 mm thickness provided by Ceraflex. Gold organometallic paste (Metalor, A1118) was used for the deposition of the counter and reference electrodes on one side of the pellet. These electrodes were deposited before the Ru catalyst deposition and were calcined in air at 650 °C for 1 h. Blank experiments have shown that gold is catalytically inactive for both the methanation and the RWGS reaction.

The Ru catalyst film was deposited on the other side of the YSZ pellet in a two step process: first, by impregnation of a $RuCl_3$ solution in *n*-propyl alcohol at 50 °C, followed by calcination in air at 500 °C for 1 h; and second, via a reduction pretreatment in 5% H_2/He at 300 °C for 1 h, for catalytic activity stabilization prior to any hydrogenation activity measurements. The resulting mass of the catalyst film was ∼3 mg.

2.2. Reactor Operation. The experiments were carried out in a continuous flow reactor, which has been thoroughly discussed previously.[40,52,53] The feed gas composition and total gas flow rate, F_t, were controlled by a set of flow meters (Brooks smart mass flow and controller B5878). Reactants were certified standards of 3% CO_2 in He and 30% H_2 in He. Pure (99.99%) He was fed to further adjust the total flow rate and the inlet gas composition at desired levels. All the experiments were performed at ambient pressure and 200 cm^3/min total volumetric gas flow rate. Feed reactant partial pressures were varied between 0.25 and 2 kPa for CO_2 and between 1 and 15 kPa for H_2. Reactants and products were analyzed by online gas chromatography in conjunction with an IR CO_2−CO−CH_4 analyzer (Fuji Electric). Constant currents and potentials were applied using an AMEL 2053 galvanostat−potentiostat. The conversion of CO_2 was usually kept below 10%.

2.3. Electrochemical Promotion Parameters Computation. The electrochemical promotion experiments were described in terms of the following two parameters, commonly used to quantify the magnitude of the EPOC effect:1. The rate enhancement ratio, ρ, defined from[40]

$$\rho = \frac{r}{r_0} \quad (5)$$

where r is the electropromoted catalytic rate and r_0 is the unpromoted rate (i.e., the open-circuit catalytic rate).2. The apparent faradic efficiency, Λ, defined from[40]

$$\Lambda_i = \frac{\Delta r_{catalytic}}{(I/F)} \quad (6)$$

where $\Delta r_{catalytic}$ is the current- or potential-induced observed change in catalytic rate (in gram equivalents per second), I is the applied current (in amperes), and F is the Faraday's constant. In this study, where CH_4 and CO were the only

dx.doi.org/10.1021/cs300072a | ACS Catal. 2012, 2, 770−780

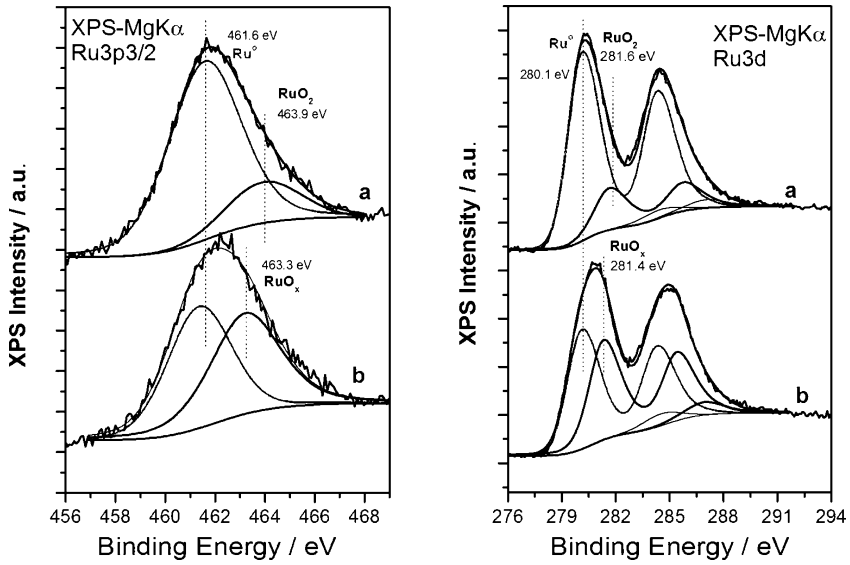

Figure 1. Ru3p3/2 (left) and Ru3d (right) spectra of the Ru/YSZ catalyst film before (a) and after (b) catalyst polarization at +1 V.

products of the CO_2 hydrogenation, the faradic efficiency for each formation reaction is defined from[40,60,61]

$$\Lambda_{CO} = \frac{2\Delta r_{CO}\ (\text{in mol/s})}{(I/F)}$$
$$\Lambda_{CH_4} = \frac{8\Delta r_{CH_4}\ (\text{in mol/s})}{(I/F)} \quad (7)$$

In the case of oxidation reactions on catalysts deposited on O^{2-} conductors, such as YSZ, a distinctive feature of electrochemical promotion is that $|\Lambda| > 1$. However, in the present case in which O_2 is not a reactant, any positive current or positive potential-induced catalytic rate change is electrochemical promotion, even when $|\Lambda| < 1$. This is not at first very clear in the case of negative current, since it might be argued that CO_2 is decomposed to CO via O^{2-} abstraction, but negative current, that is, O^{2-} removal from the catalyst, cannot lead to H_2O formation; thus again, any current or potential-induced change in catalytic rate suggests electrochemical promotion.

2.4. Catalyst Characterization by X-ray Photoelectron Spectroscopy (XPS). The ex situ photoemission experiments were carried out in an ultrahigh-vacuum system, which consists of a fast entry specimen assembly, a sample preparation, and an analysis chamber with a base pressure of $<5 \times 10^{-10}$ mbar. The system is equipped with a hemispherical electron energy analyzer (SPECS LH-10) and a dual anode, which produced the AlKα and MgKα X-ray lines. The unmonochromatized MgKα (1253.6 eV) line was used for the XPS measurements. The analyzer was working at constant pass energy (E_p = 97 eV) giving a full width at half-maximum of the main Ru3d XPS peak of 1.9 eV. The XPS core level spectra were analyzed using a fitting routine, which can decompose each spectrum into individual mixed Gaussian−Lorentzian peaks after a Shirley background subtraction. Regarding the measurement errors, for the XPS core level peaks, we estimate that for a good signal-to-noise ratio, errors in peak positions are about ±0.05 eV. Ex situ XPS spectra of the Ru catalyst were obtained both before and after electrical polarization in the electrochemical promotion (EPOC) experiments.

3. RESULTS

3.1. Catalyst Characterization. *3.1.1. SEM and X-ray Photoelectron Spectroscopy.* Scanning electron microscopy (SEM) was used to image the surface of the Ru/YSZ catalyst electrode. SEM showed that the Ru film is porous, with a thickness of ∼4 μm.

Figures 1 and 2 compare XPS spectra of the Ru catalyst film before (a) and after (b) catalyst polarization at +1 V. Thus, the spectra labeled 1a left, 1a right, and 2a were obtained before the electropromotion experiments and after a reduction pretreatment in 5% H_2/He, followed by ∼3 h exposure to the reaction mixture (7% H_2, 1% CO_2) at 220 °C. The spectra shown in the

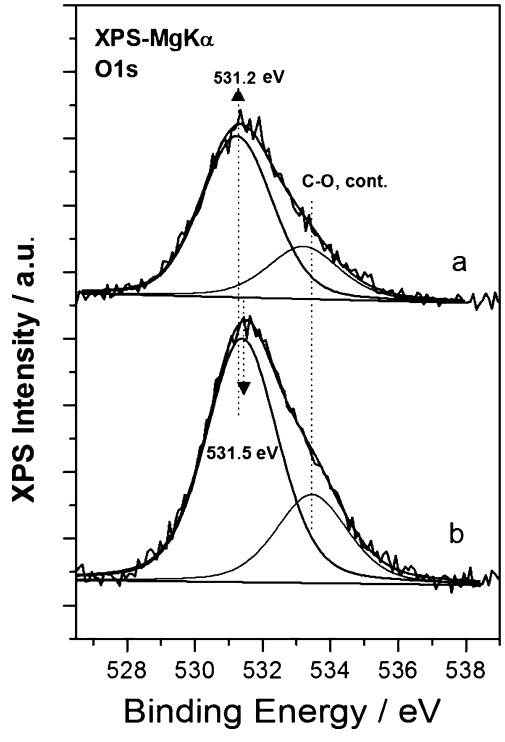

Figure 2. O1s spectra of the Ru/YSZ catalyst film before (a) and after (b) catalyst polarization at +1 V.

dx.doi.org/10.1021/cs300072a | ACS Catal. 2012, 2, 770−780

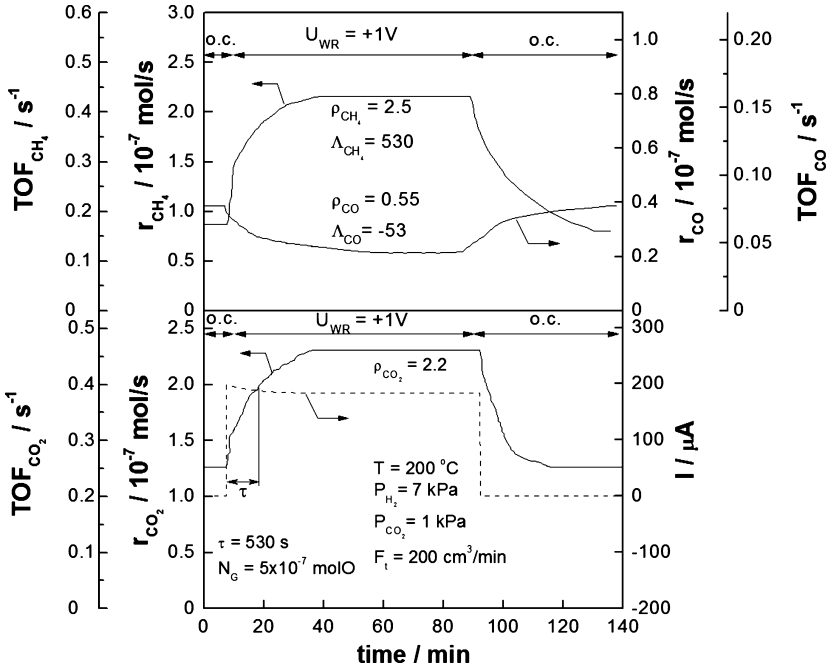

Figure 3. Transient effect of constant applied positive potential (+1 V) on the catalytic rates and TOFs of the CH_4 and CO formation and CO_2 consumption and on the current. T = 200 °C.

corresponding Figure 1b left, 1b right, and 2b were obtained with the same sample, but after previous polarization at U_{WR} = +1 V. The film was positively polarized at U_{WR} = +1 V under a 7% H_2, 1% CO_2 reaction mixture at 220 °C for 20 min and then cooled under polarization to 150 °C. Then simultaneously, current interruption, sweep with 99.99% He, and cooling to room temperature were used in an effort to avoid any changes in the state of the Ru surface state.

Ru3d is a doublet with a spin orbit splitting of 4.2 eV and intensity ratio between the Ru3d3/2 and the Ru3d5/2 components of 2:3. In the case of the catalyst film after reduction (spectrum a) the Ru3d spectrum (Figure 1 left) can be clearly analyzed into two doublets where the full width at half-maximum (fwhm) for each component is 1.9 eV. The Ru3d5/2 peak of the first doublet appears at binding energy (BE) 280.1 eV and is attributed to Ru^0, whereas the Ru3d5/2 of the second doublet appears at BE = 281.6 eV, and it is attributed to RuO_2. The intensity of the oxide component is ~4 times smaller than that of the metal. In the same spectrum, one can identify two more single peaks at 284.6 and 287.4 eV that are C1s photopeaks originating from C−C(H) and C−O species.

To verify the validity of the Ru3d analysis, the Ru3p3/2 peak was also recorded. Similarly to the Ru3d, the peak was also analyzed into two components at BEs 461.6 and 463.9 eV, representing Ru^0 and RuO_2, respectively.

Under polarization conditions, the Ru3d spectrum (spectrum b, Figure 1 left), is wider than spectrum a, and it is analyzed into two Ru3d doublets, one at BE = 280.1 eV, which represents metallic Ru, and a second one with similar intensity at BE = 281.4 eV. This BE is lower than that of the RuO_2 and possibly represents a surface oxide (RuO_x with $x < 2$), which covers the metallic Ru. Analysis of the Ru3p peak (Figure 1 right) verifies this result, since it also consists of two components with similar intensities, one representing metallic Ru and the other at 0.6 eV lower BE than that for the oxide.

It is worth noting that a peak at BE = 281.4 eV, induced in the present work via electrochemical polarization, has been also observed previously[65] in the case of thermally prepared RuO_2 films to be already present in the as-prepared sample. It is quite common, however, to find binding energy variations on the order of some dec-electron-volts between different XPS systems, mainly due to slight differences at the binding energy scale calibration. The important observation in the present work is not the exact BE value of the oxide, but the difference found between the as-prepared sample and the sample measured *at the same system* after the catalyst polarization treatment.

The O1s photopeaks for both samples consist of two components (Figure 2). The one at high BE (533.4 eV) originates from surface contaminants that include C−O functionalities. The one at low binding energy represents oxygen atoms bonded to Ru. At sample a (i.e., before polarization), the BE of these oxygen species is 531.2 eV (RuO_2). For sample b (i.e., after polarization), the binding energy of this peak is slightly higher, BE = 531.5 eV, indicating that the electron density around the oxygen atom has decreased as compared with the stoichiometric oxide.

Overall, the above observations could be attributed to the destabilization of surface Ru oxide (RuO_2) and reduction to RuO_x via lateral repulsive interactions between the backspillover O^{2-} species and the oxygen of the oxide. Over this partially reduced ruthenium state, the catalytic activity was found to be enhanced, as will be discussed later. In previous electropromotion studies of Rh/YSZ catalysts, strong kinetic support for a similar phase transition of the catalyst surface from a surface oxide to O^{2-}-covered metal upon O^{2-} supply to the catalyst surface has been demonstrated.[50,51,66] However, this is the first study in which the decomposition of surface oxide by O^{2-} supply to the catalyst surface is supported by the results of a surface spectroscopic technique.

3.1.2. Active Catalyst Surface Area. The surface area of the Ru catalyst film was estimated using the galvanostatic transient

dx.doi.org/10.1021/cs300072a | *ACS Catal.* 2012, 2, 770−780

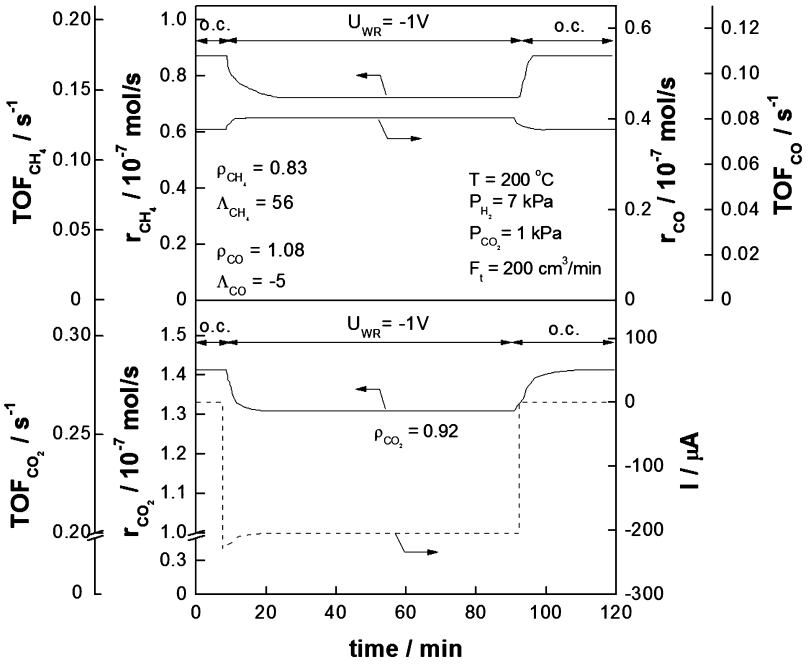

Figure 4. Transient effect of constant applied negative potential (−1 V) on the catalytic rates and TOFs of the CH_4 and CO formation and CO_2 consumption and on the current. T = 200 °C.

technique by measuring the time constant, τ, required for the rate increase, Δr, in galvanostatic electropromotion rate transients to reach 63% of its steady-state value.[40] In this way, one can estimate the reactive oxygen uptake, N_G, of the anodically polarized metal film. Assuming a 1:1 surface metal active site/O ratio, the active catalyst surface area, N_G, expressed in moles, can be computed by

$$N_G = \frac{I\tau}{2F} \tag{8}$$

during current imposition[40] or by

$$N_G = \frac{r\tau_D}{\Lambda} \tag{9}$$

during current interruption.[40] Here, r is the electropromoted rate, and the depolarization time, τ_D, defined again as the time required for the rate to decrease by 63% during depolarization, expresses the average lifetime of the backspillover $O^{\delta-}$ species originating from the YSZ lattice. Using eq 8, and the positive polarization transient at 200 °C shown in Figure 3, where τ = 530 s and I = 190 μA, one computes $N_G \approx 5 \times 10^{-7}$ mol O.

3.2. Hydrogenation Activity Measurements. Figure 3 shows the transient effect of constant positive potential application and interruption on the catalytic rates and TOFs of the formation of CH_4 and CO and of the consumption of CO_2 at 200 °C. The Figure also shows the current response. Initially, that is, before any potential application, the CO_2 consumption rate is 1.25×10^{-7} mol/s. As shown in Figure 3, positive potential (+1 V) application, that is, the O^{2-} supply to the catalyst surface, causes a significant increase in the CO_2 consumption rate, accompanied by an increase in the CH_4 formation rate and a decrease in the CO formation rate. The rate enhancement ratio was equal to 2.5 for the methanation reaction (ρ_{CH_4} = 2.5) and equal to 0.55 for the RWGS reaction (ρ_{CO} = 0.55). The apparent faradic efficiency, Λ, values were found to be 530 and −53 for the CH_4 and CO formation, respectively.

After current interruption, the catalytic rates slowly return to their initial values, indicating the reversibility of the phenomenon. On the other hand, negative potential application, that is, O^{2-} pumping from the catalyst surface, has the opposite effect, as shown in Figure 4. It causes a decrease in the methanation rate and an increase in the RGWS reaction rate. The apparent faradic efficiency values were found to be Λ_{CH_4} = 56 and Λ_{CO} = −5.

Turnover frequency, TOF_{CO_2}, values of ∼0.2 s^{-1} were found under open-circuit conditions (Figure 3 bottom), and positive potential application caused a TOF increase up to ∼0.5 s^{-1}. These values, which were calculated using $N_G = 5 \times 10^{-7}$ mol Ru, are close to those reported in the literature,[16,19,20,35,39,67] which are between 0.01 and 0.3 s^{-1} at ∼200 °C, depending on the oxide support.

The steady-state effect of temperature on the CO_2 conversion and rate of consumption and on the CH_4 and CO formation rates is shown in Figure 5, under open-circuit (o.c.) potential and under positive and negative potential applications. Under open-circuit conditions, the conversion of CO_2 increases with temperature from 5% at 200 °C to 25% at 300 °C. The effect of positive polarization on the conversion of CO_2 was significant at low temperatures (T < 250 °C) and practically vanished at 300 °C. This is probably due to the decreasing lifetime of the promoting spillover species on the catalyst surface with increasing temperature. The rate of CO formation increases monotonically with temperature, whereas a rate decrease is observed under positive polarization, as already shown in Figure 3.

The rate of CH_4 formation under open-circuit conditions exhibits a maximum at 260 °C. Under positive potential application conditions, the catalytic rate increases (electrophobic behavior), and the optimum temperature shifts to lower temperatures (220 °C).

The apparent activation energy of the methanation reaction was very small because the rate goes through a shallow

dx.doi.org/10.1021/cs300072a | ACS Catal. 2012, 2, 770−780

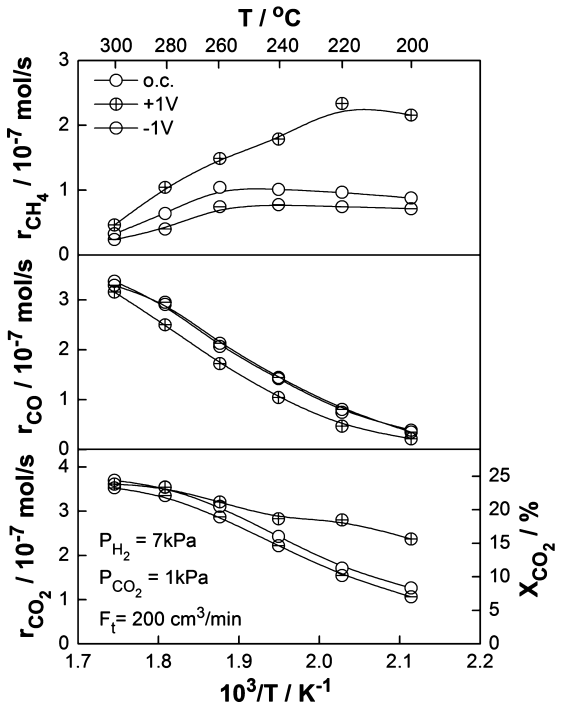

Figure 5. Arrhenius plots for the CO_2 consumption and CO and CH_4 formation under open-circuit, positive, and negative potential applications.

maximum (Figure 5), whereas the activation energy of the RWGS reaction under open-circuit conditions was ~17 kcal/mol, which is in agreement with the values reported in the literature.[10]

Figure 6 shows the steady-state effect of temperature on the selectivity to CH_4 and CO. The selectivity to CH_4, S_{CH_4} depends strongly on temperature. Under open-circuit conditions, a significant decrease in CH_4 selectivity from ~70% to

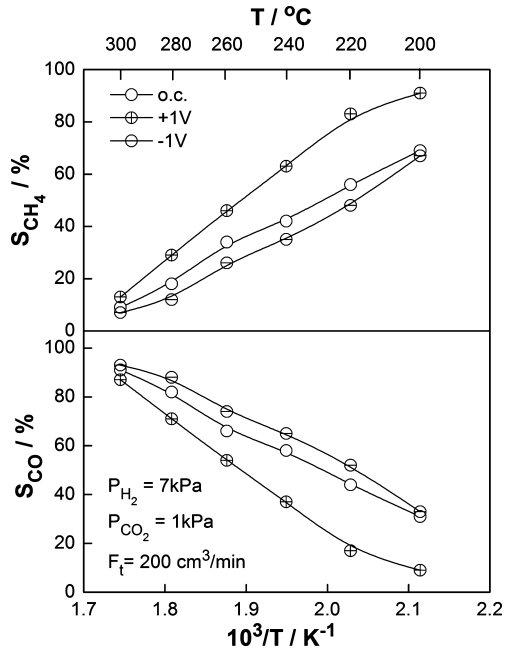

Figure 6. Steady-state effect of temperature on the selectivity to CH_4 and CO, under open-circuit and positive and negative potential applications.

~10% with temperature is observed. The major effect of polarization was observed at low temperatures, where CH_4 selectivity reached 95%. On the other hand, negative polarization caused a small decrease in CH_4 selectivity. In contrast, the selectivity to CO increased with temperature from ~30% to ~90% under open-circuit conditions.

Figure 7 shows the steady-state effect of applied potential on the catalytic formation rate and selectivity to CH_4 and CO at

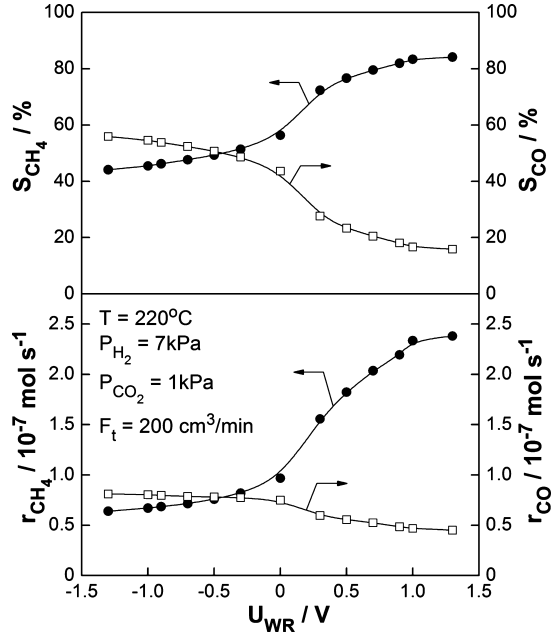

Figure 7. Steady-state effect of catalyst potential on the selectivity to CH_4 and CO. T = 220 °C.

220 °C. Under open-circuit conditions, the selectivity to CH_4 was ~56%. Positive potential application caused a monotonic increase in the selectivity, where it reached ~84% under 1.3 V. Negative potential application resulted in a decrease to ~44% under −1.3 V. In contrast, the formation rate and selectivity to CO exhibited the opposite behavior: that is, a monotonic decrease from ~58% under −1.3 V to ~18% under +1.3 V potential application.

Figure 8 (top) shows the dependence of the apparent faradic efficiency values, Λ, on the applied potential at T = 220 °C. The Λ_{CH_4} values decreased from 900 to 360 with increasing positive potential, while Λ_{CO} increased from −60 to −20. On the other hand, negative polarization caused a decrease in Λ_{CH_4} from 230 to 87 and a decrease in Λ_{CO} from −4 to −10.

Figure 8 (bottom) shows a Tafel plot (ln I vs U_{WR}) at 220 °C, where the exchange current, I_0, can be estimated by extrapolating the linear ln(I) vs U_{WR} (Tafel) part of the curves to U_{WR} = 0. The exchange current calculated by the positive and the negative potential branch was 35 μA. Using the approximate expression for the prediction of the faradic efficiency in EPOC studies,[40]

$$\Lambda_{th} = \frac{2Fr_0}{I_0} \tag{10}$$

one can calculate Λ_{th,CH_4} = 2120 for the formation of CH_4 and $\Lambda_{th,CO}$ = 320 for the formation of CO. This difference between the predicted and the experimental Λ values most likely manifests the short lifetime of the promoting species, ($O^{\delta-}$ or

dx.doi.org/10.1021/cs300072a | ACS Catal. 2012, 2, 770−780

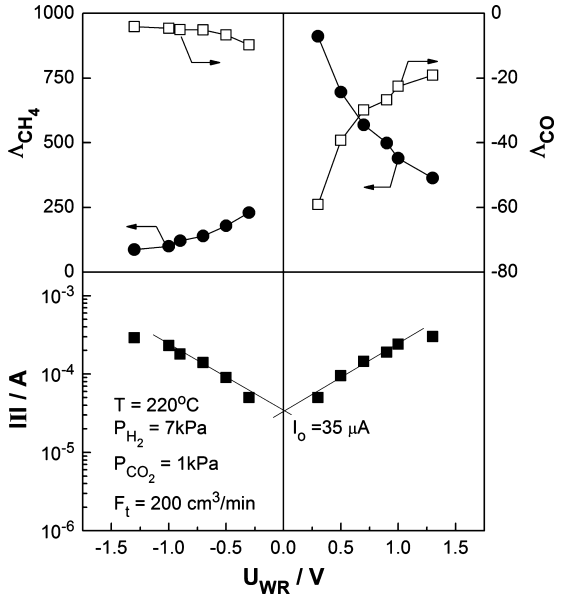

Figure 8. (top) Steady-state effect of catalyst potential on the apparent faradic efficiency values, Λ, of the methanation and the RWGS reaction. (bottom) Corresponding steady-state effect of catalyst potential on the current (Tafel plot) for the Ru/YSZ catalyst. T = 220 °C.

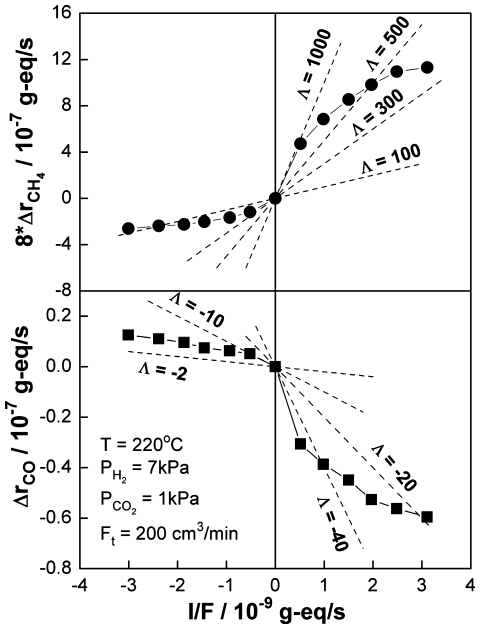

Figure 9. Effect of O^{2-} supply rate ($I > 0$) or removal rate ($I < 0$) to the Ru catalyst on the rate change of CO_2 methanation and RGWS. T = 220 °C.

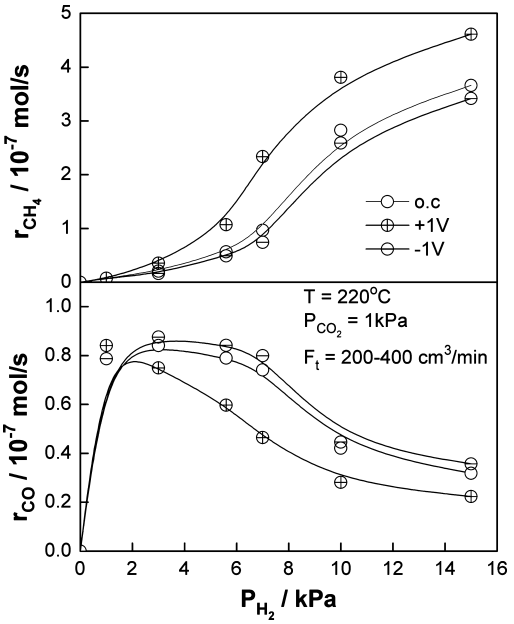

Figure 10. Steady-state effect of the H_2 partial pressure, P_{H_2}, on the rates of CO_2 methanation and RGWS reaction under open-circuit and under positive and negative potential applications. P_{CO_2} = 1 kPa, T = 220 °C.

$OH^{\zeta-}$) on the catalyst surface as a result of the strongly reducing environment. Similar deviations from eq 10 were found in the case of CO_2 hydrogenation over Cu/YSZ catalyst films.[60] It is worth noting that $|\Lambda_{CO}|$ is much smaller than Λ_{CH_4}, typically by a factor of 10. This is due to the smaller catalytic rate of the RGWS reaction, particularly under H_2 excess conditions, typically a factor of 5, than the rate of methanation.

The steady-state effect of the ionic current, I/F (g-eq/s), under polarization conditions on the potential-induced rate change of CH_4 and CO formation is shown in Figure 9. As shown in the Figure, apparent faradic efficiency values for the formation of CH_4, Λ_{CH_4}, up to 900 were obtained under positive potential application, while up to 150 under negative polarization. In the case of CO formation, apparent faradic efficiency values, Λ_{CO}, were up to −45 under positive potential application and up to −10 under negative polarization.

3.3. Kinetic Measurements. The effect of reactant partial pressure (P_{H_2} and P_{CO_2}) on the kinetics of the methanation and the RWGS reactions was investigated at 220 °C under differential conditions (i.e., with less than 10% conversion).

Figure 10 shows the dependence of the reaction rates on the partial pressure of H_2, P_{H_2}, at constant P_{CO_2}. The rate of methanation is positive order in P_{H_2} under open-circuit or positive or negative polarization, in agreement with the literature[12,19,33,35] where first-order kinetic dependence has been reported. On the other hand, the CO formation rate exhibits a negative-order dependence for P_{H_2} > 2 kPa and a weak maximum at $P_{H_2} \approx$ 2 kPa. This rate maximum possibly indicates the competitive adsorption of the reactants and the strong Ru−H bond strength, which results in high θ_H/θ_{CH_xO} values and suppresses the RWGS reaction. A similar effect occurs upon positive polarization, where the θ_H/θ_{CH_xO} ratio increases, resulting in an increase in the methanation rate.

Figure 11 shows the effect of P_{CO_2} on the intrinsic reaction rate of the methanation and the RWGS reaction, where P_{H_2} was kept constant at 7 kPa. The rate of CH_4 formation exhibits a maximum at P_{CO_2} values of ∼0.75 kPa. This maximum can be due to the θ_H/θ_{CH_xO} decrease with increasing P_{CO_2}, which suppresses the methanation reaction rate and favors the rate of the RWGS. A positive-order dependence of the methanation rate in P_{CO_2} was found in ref 67 in the range between 0.1 and 0.6 kPa. In addition, a zeroth or slightly positive-order kinetics in P_{CO_2} has been reported in the literature[19,33,35,67] for higher P_{CO_2} values. In contrast, a positive-order dependence of the RWGS

dx.doi.org/10.1021/cs300072a | ACS Catal. 2012, 2, 770−780

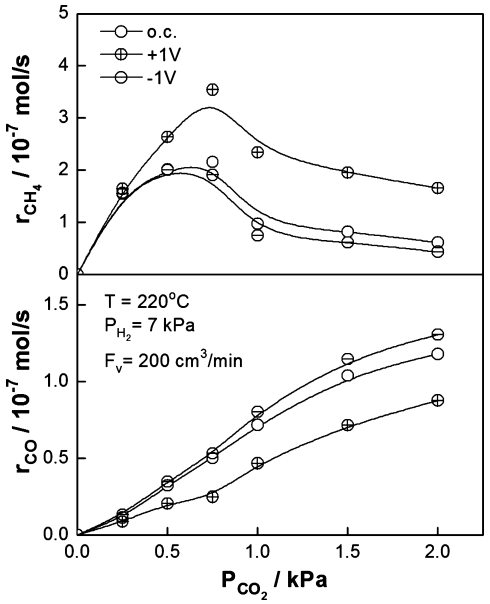

Figure 11. Steady-state effect of the CO_2 partial pressure, P_{CO_2}, on the rates of CO_2 methanation and RGWS reaction under open-circuit and positive and negative potential applications. P_{H_2} = 7 kPa, T = 220 °C.

reaction rate on P_{CO_2}, under open-circuit and positive and negative polarization conditions was found in the examined P_{CO_2} range (Figure 11), in agreement with the literature on Pt catalysts.[62]

The effect of P_{H_2} on the selectivity to CH_4 and CO is presented in Figure 12. Increasing the P_{H_2} enhances the selectivity to CH_4, which increases from ~8% at 1 kPa to ~95% at 15 kPa H_2. At the same time, the selectivity to CO_2 decreases from 92% at 1 kPa to 5% at 15 kPa.

Thus, interestingly, the effect of P_{H_2} is similar to the effect of increasing potential (Figures 6 and 12) and decreasing temperature (Figure 6).

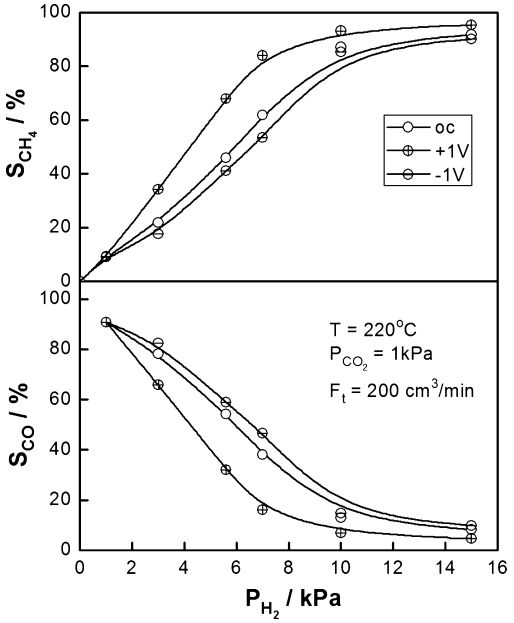

Figure 12. Steady-state effect of the H_2 partial pressure, P_{H_2}, on the selectivity to CH_4 and CO under open-circuit and positive and negative potential applications. P_{CO_2} = 1 kPa. T = 220 °C.

4. DISCUSSION

4.1. General Kinetic Features. The observed increase in the methanation rate upon positive polarization can be rationalized by (i) the decrease in RuO_2/Ru ratio, which was observed by XPS spectroscopy (shown in Figure 2a and b) and attributed to the lateral repulsive interactions between O^{2-} and oxygen of the surface RuO_2, leading to a reduced and more active Ru surface, and (ii) the concomitant increase in catalyst work function, induced by the supplied $O^{\delta-}$ promoting species to the catalytic surface and the establishment of an effective double layer on the gas-exposed Ru surface.[40] The latter results in strengthening of the Ru−H (electron donor species, D) and weakening of the Ru−CH_xO (electron acceptor species, A) bond strength and thus, in an increase in the H/CH_xO coverage ratio value (i.e., θ_H/θ_{CH_xO}), which favors the methanation reaction and suppresses the RWGS reaction, as will be discussed later on the basis of the kinetic study. At this point, it should be noted that "CH_xO" corresponds to all possible oxygen-containing intermediate compounds formed by CO_2 dissociation (x = 0, 1, 2).

After current interruption, the catalytic rates of both reactions slowly return to their initial values, as discussed above. This can be attributed to consumption of the promoting ionic species ($O^{\delta-}$ or $OH^{\zeta-}$) present on the catalytic surface by hydrogen and also to reconstruction of surface RuO_2 and subsequent return to the initial surface RuO_2/Ru ratio value by the oxygen originating from the dissociation of CO_2.

In contrast, negative polarization, that is, $O^{\delta-}$ pumping from the catalyst surface, causes a decrease in the catalyst work function[40] and a subsequent weakening of the Ru−H and strengthening of the Ru−CH_xO bond strength, which decreases the θ_H/θ_{CH_xO} ratio value and favors the RWGS reaction.

In a recent study, Bebelis et al.[64] have shown that the electrochemical supply of K^+ (an electropositive promoter) on a Pd catalyst deposited over β''-Al_2O_3, led to an increase in the RGWS reaction rate. In addition, Yaccato et al.[11] reported that Ru is the best methanizer catalyst among a variety of metals, including Rh, whereas doping with alkaline metals (electropositive promoters) was found to decrease its methanation activity. Furthermore, they reported that Na-doping of Co increased its RWGS reaction. Similar results were obtained by Hoost et al.,[39] who showed that the addition of potassium in Ru/SiO_2 resulted in a decrease in the CO methanation activity. The above results are in agreement with the present EPOC behavior, where the $O^{\delta-}$ (an electronegative promoter) supply to the surface caused at the same time an increase in the methanation and a decrease in the RGWS catalytic reaction rates.

On the basis of Figures 3 and 4 and the XPS spectra analysis in Figures 1 and 2, a schematic representation of the chemical reactions and electrochemical semireactions taking place under (a) open-circuit state and (b) positive and (c) negative polarization conditions is given in Figure 13. As shown, under open-circuit conditions (Figure 13a), RuO_2 is present on the catalyst surface (~20%), suppressing the methanation rate. Under positive polarization, RuO_2 decomposes partly to RuO_x (x < 2), and two semireactions are considered to occur at the catalyst electrode tpb: the formation of the backspillover $O^{\delta-}$ or $OH^{\zeta-}$ species (eqs 3 and 4) and the direct reaction of O^{2-} species with hydrogen to form H_2O at the tpb (eq 11).

$$O^{2-}\,(YSZ) + H_2 \rightarrow H_2O + 2e^- \qquad (11)$$

dx.doi.org/10.1021/cs300072a | ACS Catal. 2012, 2, 770−780

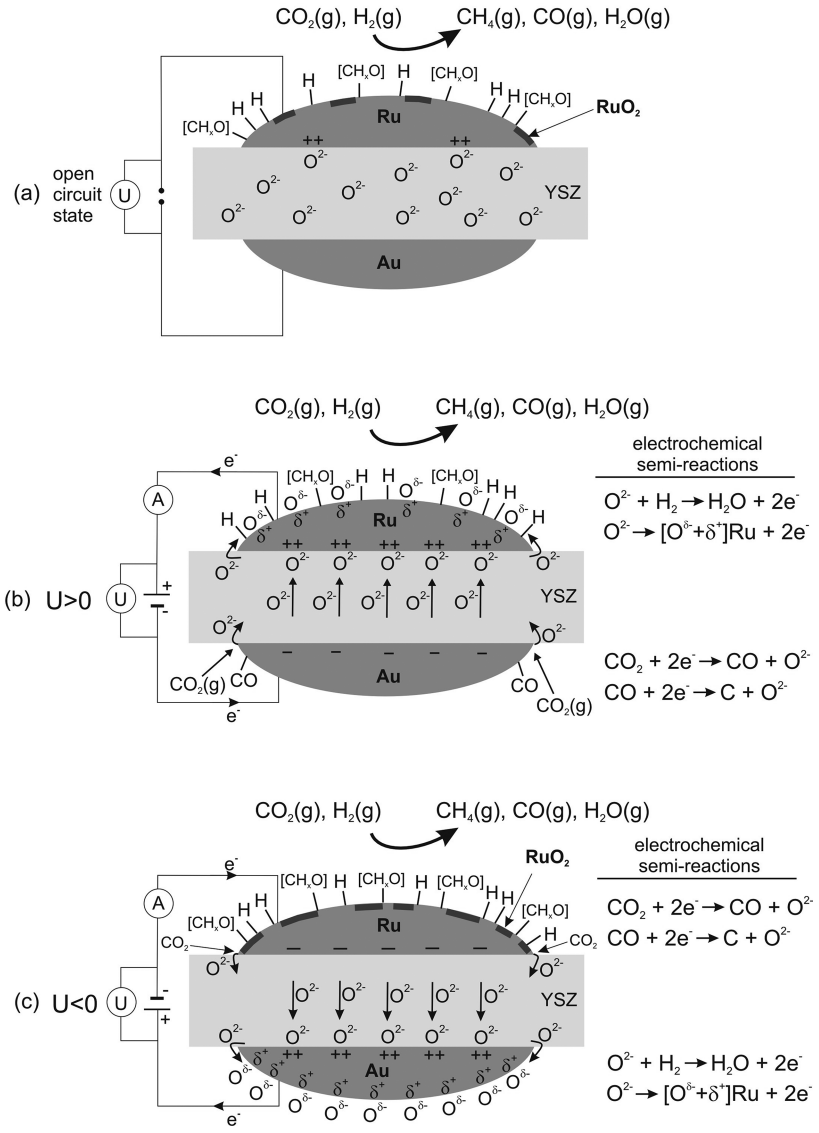

Figure 13. Schematic representation of the chemical reactions and electrochemical semireactions taking place under open-circuit (a) and positive (b) and negative (c) potential applications.

On the other hand, two semireactions are considered to take place at the gold counter electrode: the electrochemical reduction of CO_2 with the subsequent formation of CO adsorbed on the surface and the removal of O^{2-} from the catalyst to the solid electrolyte (eq 12)

$$CO_2 + 2e^- \rightarrow CO + O^{2-} \quad (12)$$

and possibly the electrochemical reduction of the adsorbed CO species (eq 13) forming surface C species.

$$CO + 2e^- \rightarrow C + O^{2-} \quad (13)$$

To support the occurrence of the above semireaction (eq 13), experiments were performed using gold for all the electrodes and feeding only CO_2 in the gas phase at 220 °C. It was found that after positive polarization in 1% CO_2/He atmosphere, treatment with O_2 resulted in the formation of small amounts of CO_2 ($\sim 10^{-9}$ mol), possibly indicating formation of carbonaceous species on gold. This is in agreement with what Kedzierzawski and Augustynski observed,[68] where formation of poisoning species on gold electrodes took place during electroreduction of CO_2. However, during normal CO_2 and H_2 feed, no blocking or poisoning effect on the current density was observed under polarization, indicating no blocking at the tpb.

Furthermore, negative potential application (Figure 13c) possibly results in the formation of surface RuO_2, and electrochemical reduction of CO_2 (or CO, or both) takes places at the tpb (eqs 12 and/or 13). At the gold counter electrode, the formation of the backspillover $O^{\delta-}$ or $OH^{\zeta-}$ species (eqs 3 and 4) or the direct reaction of O^{2-} species with hydrogen toward H_2O formation at the tpb (or both) can take place.

4.2. Comparison with the Promotional Rules. In the electrochemical promotion literature, a reaction is termed electrophobic when the rate increases with increasing catalyst potential (i.e., $\partial r\, \partial U > 0$) and electrophilic when the rate decreases with increasing catalyst potential (i.e., $\partial r\, \partial U < 0$).[40] In addition, the reaction behavior is termed volcano when the rate goes through a maximum upon varying the catalyst potential and inverted volcano when the rate goes through a minimum upon varying the catalyst potential.[40]

dx.doi.org/10.1021/cs300072a | ACS Catal. 2012, 2, 770−780

According to the promotional rules,[40,55−57] the EPOC behavior can be predicted on the basis of the open-circuit reaction kinetics with respect to the electron donor (D) and the electron acceptor (A) reactant species. An operational definition of D and A is based on whether increasing their gaseous concentration causes a decrease in catalyst potential and work function (electron donor, D) or an increase in potential and work function (electron acceptor, A).[40] Electrophobic behavior is observed for positive-order open-circuit reaction kinetics with respect to D (i.e., H_2) and negative or zeroth order kinetics with respect to A (i.e., CO_2). Electrophilic behavior is observed when the reaction kinetics are negative or zero order in D and positive order in A. When the kinetics are positive order both in D and in A, inverted volcano behavior is obtained, i.e., the rate passes through a minimum with varying catalyst potential, and volcano type behavior is observed when the rate goes through a maximum with respect to both the D and the A partial pressure. These rules are summarized in the top part of Figure 14.

As shown in the bottom part of Figure 14, all the observed potential-induced rate changes are in very good agreement with the rules of EPOC,[40,55−57] which allow for the prediction of the EPOC behavior on the basis of the kinetics of the reaction, that is, based on the measured reaction orders α_D and α_A with respect to the electron donor and electron acceptor reactant.

Figure 14 provides a confirmation of these promotional rules[40,55−57] in terms of the reaction kinetics (Figures 10 and 11) and the observed EPOC behavior (Figure 7). One observes that the methanation is always positive order in H_2 ($\alpha_D > 0$) (Figure 10). Thus, when it is negative order in CO_2 ($\alpha_A < 0$) (Figure 11, high P_{CO_2}), then electrophobic behavior is obtained; when it is positive order in CO_2 ($\alpha_A > 0$) (Figure 11, low P_{CO_2}), then inverted volcano behavior is obtained. The RWGS is always positive order in CO_2 ($\alpha_A > 0$) (Figure 11). Thus, when it is negative order in H_2 ($\alpha_D < 0$) (Figure 10, high P_{CO_2}) then electrophilic behavior is obtained; when it is positive order in H_2 ($\alpha_D > 0$) (Figure 10, very low P_{H_2}), then inverted volcano behavior is observed. One also anticipates volcano-type behavior for $\alpha_D < 0$ and $\alpha_A < 0$, that is, in the region of low temperatures and high reactant partial pressures (bottom left part of Figure 14), but no kinetic data could be obtained in that region.

5. CONCLUSIONS

The effect of electrochemical promotion of catalysis (EPOC or NEMCA effect) was investigated for the CO_2 hydrogenation reaction using Ru catalyst-electrodes over YSZ solid electrolyte pellets at temperatures of 200−300 °C and ambient pressure. Methane was found to be the main reaction product at temperatures up to 240 °C, and CO dominated at higher temperatures. Positive potential application, that is, O^{2-} promoting species supply to the Ru catalyst surface, was found to result in a significant increase in the CO_2 consumption rate, accompanied by an increase in the CH_4 and a decrease in the CO formation rates. This change in the product formation rates causes a significant increase in the reaction selectivity to CH_4. The opposite effect was observed by negative potential application, that is, O^{2-} species removal from the catalyst surface. The results are in agreement with the rules of electrochemical and classical promotion of catalysis.

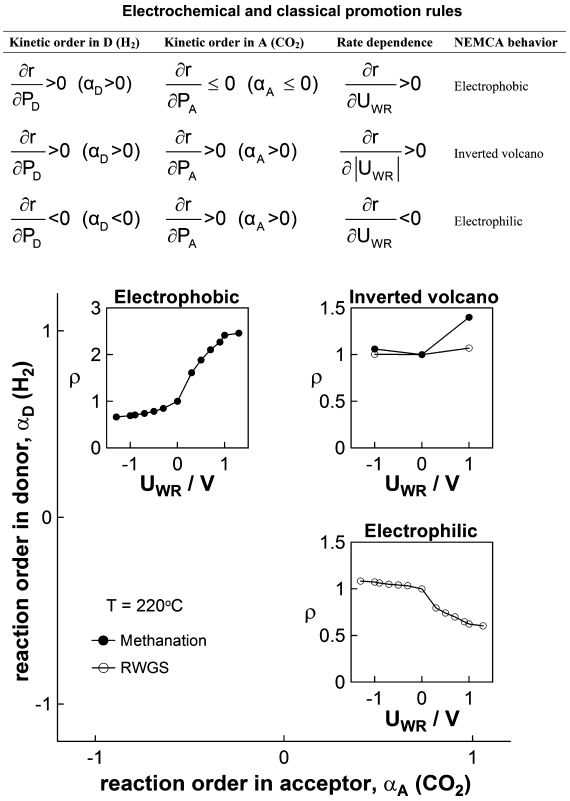

Figure 14. Promotional rules[40,55−57] (top) and their confirmation (bottom). "D" denotes an electron donor adsorbate (i.e., one which decreases the catalyst potential or work function; e.g., H_2), "A" denotes an electron acceptor adsorbate (i.e., one that increases catalyst potential and work function); α_D and α_A are the kinetic reaction orders of the rate with respect to D and A. The confirmation is based on Figures 10, 11 and 7 (bottom). The methanation is always positive order in H_2 ($\alpha_D > 0$) (Figure 10). Thus, when it is negative order in CO_2 ($\alpha_A < 0$) (Figure 11, high P_{CO_2}), then electrophobic behavior is obtained; when it is positive order in CO_2 ($\alpha_A > 0$) (Figure 11, low P_{CO_2}), then inverted volcano behavior is obtained. The RWGS is always positive order in CO_2 ($\alpha_A > 0$) (Figure 11). Thus, when it is negative order in H_2 ($\alpha_D < 0$) (Figure 10, high P_{H_2}), then electrophilic behavior is obtained; when it is positive order in H_2 ($\alpha_D > 0$) (Figure 10, very low P_{H_2}), then inverted volcano behavior is obtained.

AUTHOR INFORMATION

Corresponding Author

*E-mails: souentie@chemeng.upatras.gr; cgvayenas@upatras.gr.

Notes

The authors declare no competing financial interest.

ACKNOWLEDGMENTS

The authors are thankful to the Greek Ministry of Development, GSRT (Project Synergasia 09SYN-42-729), for financial support. We are also very thankful to our two reviewers for their excellent suggestions.

REFERENCES

(1) Abe, T.; Tanizawa, M.; Watanabe, K.; Taguchi, A. *Energy Environ. Sci.* **2009**, *2*, 315−321.
(2) Falconer, J. L.; Zağli, A. E. *J. Catal.* **1980**, *62*, 280−285.
(3) Gupta, N. M.; Kamble, V. S.; Kartha, V. B.; Iyer, R. M.; Thampi, K. R.; Gratzel, M. *J. Catal.* **1994**, *146*, 173−184.

(4) Lapidus, A. L.; Gaidai, N. A.; Nekrasov, N. V.; Tishkova, L. A.; Agafonov, Y. A.; Myshenkova, T. N. *Pet. Chem.* **2007**, *47*, 75−82.
(5) Marwood, M.; Doepper, R.; Renken, A. *Appl. Catal., A* **1997**, *151*, 223−246.
(6) Román-Martínez, M. C.; Cazorla-Amorós, D.; Linares-Solano, A.; Salinas-Martínez de Lecea, C. *Appl. Catal., A* **1996**, *134*, 159−167.
(7) Schild, C.; Wokaun, A.; Baiker, A. *J. Mol. Catal.* **1990**, *63*, 243−254.
(8) Vesborg, P. C. K.; Chorkendorff, I.; Knudsen, I.; Balmes, O.; Nerlov, J.; Molenbroek, A. M.; Clausen, B. S.; Helveg, S. *J. Catal.* **2009**, *262*, 65−72.
(9) Clarke, D. B.; Bell, A. T. *J. Catal.* **1995**, *154*, 314−328.
(10) Wei, W.; Jinlong, G. *Front. Chem. Sci. Eng.* **2011**, *5*, 2−10.
(11) Yaccato, K.; Carhart, R.; Hagemeyer, A.; Lesik, A.; Strasser, P.; Volpe, A. F. Jr; Turner, H.; Weinberg, H.; Grasselli, R. K.; Brooks, C. *Appl. Catal., A* **2005**, *296*, 30−48.
(12) Scirè, S.; Crisafulli, C.; Maggiore, R.; Minicò, S.; Galvagno, S. *Catal. Lett.* **1998**, *51*, 41−45.
(13) Karelovic, A.; Ruiz, P. *Appl. Catal., B* **2011**, in Press.
(14) Fisher, I. A.; Bell, A. T. *J. Catal.* **1996**, *162*, 54−65.
(15) Park, J.-N.; McFarland, E. W. *J. Catal.* **2009**, *266*, 92−97.
(16) Solymosi, F.; Erdohelyi, A.; Kocsis, M. *J. Chem. Soc., Faraday Trans. 1: Phys. Chem. Condens. Phases* **1981**, *77*, 1003−1012.
(17) Eckle, S.; Anfang, H. G.; Behm, R. J. *J. Phys. Chem. C* **2011**, *115*, 1361−1367.
(18) Hori, Y.; Takahashi, I.; Koga, O.; Hoshi, N. *J. Mol. Catal A: Chem.* **2003**, *199*, 39−47.
(19) Prairie, M. R.; Highfield, J. G.; Renken, A. *Chem. Eng. Sci.* **1991**, *46*, 113−121.
(20) Li, D.; Ichikuni, N.; Shimazu, S.; Uematsu, T. *Appl. Catal., A* **1998**, *172*, 351−358.
(21) Omae, I. *Catal. Today* **2006**, *115*, 33−52.
(22) Weatherbee, G. D.; Bartholomew, C. H. *J. Catal.* **1984**, *87*, 352−362.
(23) Amenomiya, Y. *Appl. Catal.* **1987**, *30*, 57−68.
(24) Brown Bourzutschky, J. A.; Homs, N.; Bell, A. T. *J. Catal.* **1990**, *124*, 73−85.
(25) Gogate, M. R.; Davis, R. J. *Catal. Commun.* **2010**, *11*, 901−906.
(26) Riedel, T.; Schaub, G.; Jun, K. W.; Lee, K. W. *Ind. Eng. Chem. Res.* **2001**, *40*, 1355−1363.
(27) Sahibzada, M.; Chadwick, D.; Metcalfe, I. S. *Catal. Today* **1996**, *29*, 367−372.
(28) Takeishi, K.; Yamashita, Y.; Aika, K.-i. *Appl. Catal., A* **1998**, *168*, 345−351.
(29) Mills, G. A.; Steffgen, F. W. *Catal. Rev.* **1974**, *8*, 159−210.
(30) Rodríguez-Ramos, I.; Reinoso, F. R.; Guerrero-Ruiz, A.; de Dios López-González, J. *J. Chem. Technol. Biotechnol.* **1986**, *36*, 67−73.
(31) Andersson, M. P.; Abild-Pedersen, F.; Remediakis, I. N.; Bligaard, T.; Jones, G.; Engbæk, J.; Lytken, O.; Horch, S.; Nielsen, J. H.; Sehested, J.; Rostrup-Nielsen, J. R.; Nørskov, J. K.; Chorkendorff, I. *J. Catal.* **2008**, *255*, 6−19.
(32) Weatherbee, G. D.; Bartholomew, C. H. *J. Catal.* **1982**, *77*, 460−472.
(33) Marwood, M.; Doepper, R.; Prairie, M.; Renken, A. *Chem. Eng. Sci.* **1994**, *49*, 4801−4809.
(34) Dubé, P.; Brisard, G. M. *J. Electroanal. Chem.* **2005**, *582*, 230−240.
(35) Prairie, M. R.; Renken, A.; Highfield, J. G.; Ravindranathan Thampi, K.; Grätzel, M. *J. Catal.* **1991**, *129*, 130−144.
(36) Liotta, L. F.; Martin, G. A.; Deganello, G. *J. Catal.* **1996**, *164*, 322−333.
(37) Boffa, A.; Lin, C.; Bell, A. T.; Somorjai, G. A. *J. Catal.* **1994**, *149*, 149−158.
(38) Erdöhelyi, A.; Pásztor, M.; Solymosi, F. *J. Catal.* **1986**, *98*, 166−177.
(39) Hoost, T. E.; Goodwin, J. G. Jr. *J. Catal.* **1992**, *137*, 22−35.
(40) Vayenas, C. G.; Bebelis, S.; Pliangos, C.; Brosda, S.; Tsiplakides, D. *Electrochemical Activation of Catalysis: Promotion, Electrochemical Promotion, and Metal-Support Interactions*; Kluver Academic/Plenum Plublishers: New York, 2001.
(41) Stoukides, M.; Vayenas, C. G. *J. Catal.* **1981**, *70*, 137−146.
(42) Vayenas, C. G.; Bebelis, S.; Ladas, S. *Nature* **1990**, *343*, 625−627.
(43) Politova, T. I.; Sobyanin, V. A.; Belyaev, V. D. *React. Kinet. Catal. Lett.* **1990**, *41*, 321−326.
(44) Lambert, R. In Wieckowski, A., Savinova, E.R., Vayenas, C.G., Eds.; *Catalysis and Electrocatalysis at Nanoparticle Surfaces*; Marcel Dekker, Inc.: New York, 2003.
(45) Kokkofitis, C.; Karagiannakis, G.; Zisekas, S.; Stoukides, M. *J. Catal.* **2005**, *234*, 476−487.
(46) Kotsionopoulos, N.; Bebelis, S. *J. Appl. Electrochem.* **2005**, *35*, 1253−1264.
(47) Poulidi, D.; Thursfield, A.; Metcalfe, I. S. *Top. Catal.* **2007**, *44*, 435−449.
(48) Cavalca, C. A.; Larsen, G.; Vayenas, C. G.; Haller, G. L. *J. Phys. Chem.* **1993**, *97*, 6115−6119.
(49) Li, X.; Gaillard, F.; Vernoux, P. *Top. Catal.* **2007**, *44*, 391−398.
(50) Baranova, E. A.; Thursfield, A.; Brosda, S.; Fóti, G.; Comninellis, C.; Vayenas, C. G. *Catal. Lett.* **2005**, *105*, 15−21.
(51) Baranova, E. A.; Thursfield, A.; Brosda, S.; Fóti, G.; Comninellis, C.; Vayenas, C. G. *J. Electrochem. Soc.* **2005**, *152*, E40−E49.
(52) Katsaounis, A. *J. Appl. Electrochem.* **2010**, *40*, 885−902.
(53) Vayenas, C. G.; Koutsodontis, C. G. *J. Chem. Phys.* **2008**, *128*, 182506.
(54) de Lucas-Consuegra, A.; Dorado, F.; Jiménez-Borja, C.; Caravaca, A.; Vernoux, P.; Valverde, J. L. *Catal. Today* **2009**, *146*, 293−298.
(55) Brosda, S.; Vayenas, C. G.; Wei, J. *Appl. Catal., B* **2006**, *68*, 109−124.
(56) Vayenas, C. G.; Brosda, S.; Pliangos, C. *J. Catal.* **2001**, *203*, 329−350.
(57) Vayenas, C. G.; Brosda, S.; Pliangos, C. *J. Catal.* **2003**, *216*, 487−504.
(58) Souentie, S.; Lizarraga, L.; Kambolis, A.; Alves-Fortunato, M.; Valverde, J. L.; Vernoux, P. *J. Catal.* **2011**, *283*, 124−132.
(59) Thursfield, A.; Brosda, S.; Pliangos, C.; Schober, T.; Vayenas, C. G. *Electrochim. Acta* **2003**, *48*, 3779−3788.
(60) Papaioannou, E. I.; Souentie, S.; Hammad, A.; Vayenas, C. G. *Catal. Today* **2009**, *146*, 336−344.
(61) Bebelis, S.; Karasali, H.; Vayenas, C. G. *J. Appl. Electrochem.* **2008**, *38*, 1127−1133.
(62) Pekridis, G.; Kalimeri, K.; Kaklidis, N.; Vakouftsi, E.; Iliopoulou, E. F.; Athanasiou, C.; Marnellos, G. E. *Catal. Today* **2007**, *127*, 337−346.
(63) Jiménez, V.; Jiménez-Borja, C.; Sánchez, P.; Romero, A.; Papaioannou, E. I.; Theleritis, D.; Souentie, S.; Brosda, S.; Valverde, J. L. *Appl. Catal., B* **2011**, *107*, 210−220.
(64) Bebelis, S.; Karasali, H.; Vayenas, C. G. *Solid State Ionics* **2008**, *179*, 1391−1395.
(65) Rochefort, D.; Dabo, P.; Guay, D.; Sherwood, P. M. A. *Electrochim. Acta* **2003**, *48*, 4245−4252.
(66) Constantinou, I.; Archonta, D.; Brosda, S.; Lepage, M.; Sakamoto, Y.; Vayenas, C. G. *J. Catal.* **2007**, *251*, 400−409.
(67) Kowalczyk, Z.; Stołecki, K.; Raróg-Pilecka, W.; Miśkiewicz, E.; Wilczkowska, E.; Karpiński, Z. *Appl. Catal., A* **2008**, *342*, 35−39.
(68) Kedzierzawski, P.; Augustynski, J. *J. Electrochem. Soc.* **1994**, *141*, L58−L60.